The effect of global and regional solar shading on climate: A simulation study

E. Agyemang-Oko [1,2], H. Yang [2], S. Xiaoxu [2], G. Lohmann [1,2]

[1]Climate Sciences, Alfred Wegener Institute, Helmholtz Centre for Polar and Marine Research, Bremerhaven, Germany
[2]Institute of Environmental Physics, University of Bremen, Bremen, Germany
[1]Klussmannstr. 3, 27570 Bremerhaven Germany
[2]Bibliothekstrasse 1 28359 Bremen Germany

Corresponding author: ernest1@uni-bremen.de, (EA-O)

Abstract

The potential climate impact of solar geoengineering is examined using climate model simulations by artificially reducing the incoming solar radiation at the top of the atmosphere. Climate scenario simulations indicate that a doubling of atmospheric carbon dioxide ($2xCO_2$) induces a surface temperature rise which is amplified over the poles primarily during the respective winter. The warming also causes intensification and poleward shift of the global precipitation pattern. In our model, a 2.1% globally uniform solar reduction can largely compensate the global mean warming caused by a doubling of CO_2. We find that solar shading is efficient to restore the temperature at the region where the background sunshine is strong, regionally at low-latitudes, seasonally during summer. Solar shading would lead to an overall weakening of the global hydrological cycle, resulting in a large-scale drought. A 3.6% solar reduction in the tropics can largely reduce the tropical and global warming as well. However, it reduces the precipitation at the central tropics, while increase the precipitation over the monsoon region. Comparatively, a 14% solar reduction over the poles can effectively prevent the polar summer temperature increase and sea-ice retreat. However, caused by the increased temperature gradient, polar solar shading increases the storm activity at high-latitudes, especially during summer when the solar reduction reaches its maximum amplitude. Our simulations show that solar shading could be an effective way to stabilize the polar cryosphere. Nevertheless, it has a strong impact on the hydrological cycle and provides a heterogenous regional climate signal.

Keywords Climate Engineering; Global warming; Climate Model; Solar shading.

1 Introduction

Global warming due to greenhouse gas emissions have increased and emerged as one of the biggest environmental challenges facing the world. Its effects have been evident for many years and will become more severe in the coming decades (Van Aalst, 2006). During the Paris Climate Change Agreement in 2015, world's nations agreed to strengthen efforts to limit the global temperature rises to well below 2°C above the pre-industrial level by 2100. Regardless of this ambition, it is unlikely to stay within 2°C limit as anthropogenic emissions of greenhouse gases continue increasing which have caused radiative imbalance at the top of the atmosphere (TOA).

A reduction in greenhouse gas concentrations in the atmosphere remains the only permanent method to address climate change. However, efforts to mitigate climate change by reducing the emissions are still challenging. This has led to an interest in climate engineering (Crutzen, 2006) which has recently gained attention as a way to manage climate by artificially cooling the planet. There are two primary categories of climate engineering (Caldeira et al., 2013): Carbon Dioxide Removal methods and solar geoengineering (also known as Solar Radiation Management). The carbon dioxide removal methods seek to reduce the CO_2 content in the atmosphere, while solar geoengineering intent to reflect more sunlight back into space using various approaches, such as injecting reflecting aerosol particles (Crutzen, 2006; Ban-Weiss & Caldeira, 2010; McClellan et al., 2012) and placing sunshade between the Earth and the Sun (Angel, 2006; Lunt et al., 2008). Solar geoengineering has suggested to be as a possible intermediate solution to gain time for a proper long-term strategy to reduce global warming (Council, 2015; P. J. Irvine et al., 2016).

Modelling studies have been performed using solar geoengineering schemes in which uniform percentage of incoming solar radiation was reduced to compensate the atmospheric CO_2 induced warming (Govindasamy & Caldeira, 2000; Govindasamy et al., 2002, 2003; Caldeira & Wood, 2008; Kravitz et al., 2013, 2014; Kalidindi et al., 2015). They demonstrate that solar geoengineering could partly compensate global and annual mean surface temperature changes caused by an elevated atmospheric CO_2 content. Solar shading might take less time to have an impact on the climate system, as the climate reacts quickly to a reduction in solar radiation (Matthews & Caldeira, 2007; Shepherd, 2009). However, reduction in insolation would affect the global hydrological cycle (Govindasamy et al., 2003; Bala et al., 2008; Caldeira & Wood, 2008; Ban-Weiss & Caldeira, 2010; Kravitz et al., 2013), extreme events (Curry et al., 2014), vegetation pattern (Naik et al., 2003; Glienke et al., 2015) and other side effects (P. J. Irvine et al., 2016). Given that global warming results in distinct climate impacts at different regions, global uniform solar shading may not be the suitable approach.

To explore the impacts of global and regional shading, we compare results from three model simulations: pre-industrial (piControl), doubling of the atmospheric CO_2 content ($2\times CO_2$) and idealized solar geoengineering implemented globally and regionally to compensate the radiative impacts of CO_2.

2 Model and Methods

2.1 AWI Earth System Model (AWI-ESM)

The Alfred Wegener Institute Earth System Model (AWI-ESM), (Sidorenko et al., 2019) is used to perform the simulations of this study. The AWI-ESM was developed by the Alfred Wegener Institute, Helmholtz Centre for Polar and Marine Research. It consists of the atmospheric model ECHAM6 and the Finite Element Sea ice-Ocean Model (FESOM) (Wang et al., 2014; Danilov et al., 2017). The simulations conducted in this study used the AWI-ESM with atmosphere resolution of 1.875×1.875 degree (approximately 200 km near equator). Ocean and sea ice were simulated on a mesh with resolution varying from nominal one degree in the interior of the ocean to relatively high resolution (up to 24 km) in the equatorial belt and over high latitudes. AWI-ESM has previous widely applied in the simulations of paleo, present and future climates (Lohmann et al., 2020; Shi et al., 2020; Kageyama et al., 2021; Brierley et al., 2020; Yang, Lohmann, Krebs-Kanzow, et al., 2020).

2.2 Experimental Design

We perform three sets of simulations. Firstly, a pre-industrial control simulation is carried out under the pre-industrial CO_2 (i.e., 284 ppmv) forcing and normal amount of incoming solar flux (sunshine) of 1360.744 Wm^{-2}. It is denoted as piControl simulation and integrated for 1200 years. The last 100 years results are used to represent the climate condition without anthropogenic global warming. To obtain the pattern of anthropogenic climate change, we run another experiment, namely, the $2\times CO_2$ experiment, in which the atmospheric CO_2 concentration is instantaneously doubled from the piControl level with normal amount of incoming solar flux. This experiment is initialized from the 1100th model year of the piControl experiment. To evaluate the impact of solar shading on climate, we conducted three additional experiments in which a uniform reduction of the incoming solar radiation globally and regionally over the tropics (between 30°S-30°N) and the poles (higher than 60°N/S) is applied (as listed in Table 1). In the three simulations, the greenhouse gas forcing is kept identical to the $2\times CO_2$ experiment.

Depending on the model, different percentages (1.75-2.5%) of solar reduction are required to fully compensate the surface warming induced by doubling of CO_2 (Govindasamy et al., 2003; Caldeira & Wood, 2008; Kravitz et al., 2013). Sensitivity tests with our model indicate that a global 2.1% solar radiation reduction is approximately the value needed to offset the global mean temperature rise of the doubling CO_2 concentration in the atmosphere. Besides the globally uniform 2.1% solar radiation experiment (Global2.1), two shading simulations focusing on the tropics and the polar regions are performed. Experiment Tropical3.6 serves to stabilize the tropical climate, while Polar14 is designed to keep the polar temperatures low to avoid an instability of the polar ice sheets and associated potential irreversible sea level rise (Applegate & Keller, 2015; McCusker et al., 2015; P. J. Irvine et al., 2009). The 2×CO_2 simulation and the shading simulations were run for 200 model years with the last 100 years being used to compute climate anomalies.

3 Results

3.1 Climate with doubling of atmospheric carbon dioxide (2×CO_2)

3.1.1 Surface Air Temperature

Fig. 1 shows the surface air temperature anomalies in the 2×CO_2 simulation. In general, surface warming is detected in all regions in both annual and seasonal perspectives. The 2×CO_2 simulation shows a global mean surface air temperature rise of 2.12°C after 100 years. The annual mean temperature anomalies show strongest positive anomalies at high latitudes (Fig. 1). The surface air temperature anomalies are significantly different in summer and winter. At high latitudes, the doubling CO_2 simulation shows a pronounced warming during winter. This leads to a reduction in temperature seasonality, induced by feedback processes (Lee, 2014; Dai et al., 2019). The temperature increase is stronger over land than over the ocean due to the different heat capacities (Sutton et al., 2007; Joshi et al., 2008; Boer, 2011).

3.1.2 Precipitation

The 2×CO_2 simulation shows a significant increase in global mean precipitation of 3.63±0.41% (Table 2) with a strong spatial inhomogeneous pattern (Fig. 2). There are significant positive anomalies over the Intertropical Convergence zone (ITCZ) and at high latitudes, but significant negative anomalies in the subtropics and some tropical areas. This precipitation anomaly pattern reinforces the background hydrological cycle, which was described as "dry gets drier, wet gets wetter", as a result of intensified hydrological cycle. Comparing the zonal mean precipitation anomaly to the climatological distribution of precipitation reveals a poleward shift of precipitation pattern, as seen by the peak increase/decrease of precipitation at the polar flanks of the climatology peak maximum/minimum precipitation. Such precipitation pattern shift is partly associated poleward shift of oceanic and atmospheric circulation (Hu & Fu, 2007; Lu et al., 2007; Yang et al., 2022), as a result of migration in meridional temperature gradients (Yang, Lohmann, Lu, et al., 2020). The seasonal precipitation anomaly is very similar to the annual precipitation change, however with stronger amplitudes.

3.1.3 Sea Ice

The sea ice coverage over the Arctic Ocean decreases substantially in September with only a little ice found around the central and western Arctic near the Canadian Archipelago. The reduction in Arctic sea ice is particularly pronounced in the Eastern Siberian, the Canadian Archipelago, the Chukchi and Beaufort Seas, and around Greenland. The sea-ice extent appears to be regrown during the following winter (March) with a little reduction over the Eurasian side of the Arctic Ocean and the subpolar North Atlantic Ocean. With this warmer climate, the Arctic will lose much of its ability to reflect incoming sunlight back to space without the summer sea ice. This causes an Arctic amplification of temperature changes (Lee, 2014; Dai et al., 2019). The reduction in Antarctic late summer (March) sea ice is pronounced all over the Southern Ocean, with little ice left close to the Antarctic Peninsula on the Weddell Sea. The most pronounced reduction in September ice occurs in the Indian Ocean sector. The heat exchange between the upper ocean and the atmosphere is expected to be stronger with a reduced polar sea ice coverage (Tietsche et al., 2011).

3.2 Global Uniform Solar Radiation Management

3.2.1 *Surface Air Temperature*

We find that a reduction in solar radiation by 2.1% compensates the warming induced by 2×CO_2. As shown in Fig. 4, 2.1% uniform solar radiation reduction largely compensates the global annual mean warming from the doubling atmospheric CO_2 warming (Fig. 1 and Table 2). However, shading causes spatial and seasonal temperature anomaly patterns different to increased CO_2 which is due to different spatio-temporal distribution of the radiative forcing (MacMartin et al., 2018).

There is a decrease in surface air temperature in the tropics and subtropics, mostly over the oceans. In contrast, residual warmings with an amplitude of about 1-2°C are found at high latitudes. This is due to the fact that Global2.1 produces the strongest net solar reduction at low latitudes, where strong background solar radiation exists. Comparably, residual warmings over the high latitudes are predominantly observed during winter, when background solar radiation is weak. Our results suggest that global uniform percentage of solar reduction is effective at reducing warming over regions with high background sunlight, seasonally during summer, and regionally at low latitudes.

3.2.2 *Precipitation*

Reduction in solar radiation causes an overall reduction (-1.29±0.38%) in the global mean hydrological cycle compared to the global net precipitation in piControl. A previous study also noticed this reduction in precipitation, as a result of larger sensitivity of evaporation response to solar forcing than CO_2 forcing (Bala et al., 2008). Interestingly, the most prominent precipitation reduction is found over the ocean centred around the ITCZ (Roose et al., 2023). In contrast, on the land, precipitation has slightly increased. This is due to more residual warming over land than over the ocean (Fig. 4), which enhances the land-sea temperature contrast and monsoon precipitation. Our results indicate that residual warming should be preserved in order to maintain the global mean precipitation.

3.3 Tropical Solar Radiation Management

3.3.1 *Surface Air Temperature*

The tropics receive the highest amount of solar radiation, resulting in surface temperatures over 30°C. Under anthropogenic-induced warming, increased temperatures and humidity threaten the habitability of the tropics where more than 40% of the world's population lives (CIESIN, 2015; Y. Zhang et al., 2021). This promotes ideas for tropical shading with a solar radiation reduction over the tropics. We find that a 3.6% tropical solar reduction is equivalent to a globally uniform 2.1% solar reduction (Table 2). Regionally, Tropical3.6 shows an over-cooling (less than 1 K) in the tropics, but a residual warming (around 1-2 K) at high latitudes, where the solar reduction is not applied. Similar to Global2.1, the high-latitude residual warming is primarily found during winter. This results in a weaker equator-to-pole temperature gradient during winter.

3.3.2 *Precipitation*

As in Global2.1, solar shading at low latitudes reduces (-0.95±0.42%, Table 2) the global mean hydrological cycle, relative to piControl. Prominent precipitation reductions are found near the ITCZ in all seasons (Fig. 7). This precipitation reduction is due the fact that the strongest solar reduction occurs there, reducing the available energy for developing deep atmospheric convection. In contrast to the tropical shading, an increase of precipitation is found in the subtropical monsoon regions, such as Northern Africa, India, East Asia, the Atlantic coast of North America, Brazil, Australian and Southern

Africa. This specific land-sea distribution, combined with solar reduction over the tropics, contributes to an increase in land-sea temperature contrast (Fig. 6) and monsoon precipitation over the subtropical area.

3.4 Polar Solar Radiation

Global warming induces dramatic warming over the polar regions. This amplified polar warming is a potential cause for irreversible disintegrations of the Greenland and Antarctic Ice sheets, which are critical for the future sea level rise (Moore et al., 2010). Polar sea-ice melt amplifies the warming through the ice-albedo feedback. Therefore, reducing solar over polar regions appears to be more efficient in mitigating anthropogenic-induced high-latitude warming. Moreover, the polar regions are relatively sparsely populated and have 24 hours sunlight in summer. Considering all these facts, we designed another experiment to compensate for warming by reducing the incoming sunlight over the polar regions (poleward of 60° at the Northern and Southern Hemispheres). We find that a 28% polar shading corresponds to a global solar reduction of 2.1%. However, we see that this leads to a very cold climate in the polar regions. Therefore, we have performed a simulation with 14% solar reduction in the polar region, namely the Polar14 experiment.

3.4.1 Surface Air Temperature

Polar14 reduces the global mean surface air temperature from the abrupt $2\times CO_2$ simulation by around 1 K (Table 2). In the annual mean perspective, the Polar14 compensates most of the high-latitude warming caused by the doubling $2\times CO_2$ warming (Fig. 1), with an over-cooling in summer but residual warming in winter (Fig. 8). This might prevent the surface melting during summer. We also expect that Polar14 can reduce the risk of Antarctic Ice Sheet disintegration, as regional cooling is simulated at the margin of the Antarctic Ice Sheet. Due to the oceanic and atmospheric heat transport, the 14% reduction in polar regions reduce tropical warming as compared to the $2\times CO_2$ simulation (Fig. 1), despite the fact that the shading is applied only at the polar regions.

3.4.2 Increase storms under polar geoengineering

A Reduction of solar radiation in the polar regions leads to a stronger equator-to-pole temperature gradient, especially at the edge of where solar reduction is applied. Fig. 9 shows the eddy kinetic energy (EKE) anomaly, which is an indicator of storm activity. Polar14 could lead to stronger and more frequent storms at the polar regions, especially in summer when the actual solar reduction is maximum.

3.4.3 Sea Ice

The patterns of the mean Arctic and Antarctic sea ice cover in the polar shading are shown in Fig. 10. Polar14 compensates most of the $2\times CO_2$ summer warming in the polar regions, so that the summer sea-ice extent is close to the piControl level. However, shading has less impact on the winter sea ice. With the reduction in solar radiation in Polar14, the albedo of the ocean will increase significantly, leading to a reduction in the absorption of shortwave as sea ice cover returns to pre-industrial levels, resulting in less release of latent heat from the ocean to the atmosphere.

4 Discussion

Climate model simulations have been performed in which the solar irradiance is uniformly reduced by a certain percentage to offset the warming caused by increased atmospheric CO_2. Our results, which are consistent with previous studies suggest that shading could reduce global warming. Although such mitigation can help to reduce temperature, it could lead to undesirable side-effects (Z. Zhang et al., 2015). Numerical climate model simulations have consistently indicated that SRM not only reduces the Earth's temperature but also affects the precipitation pattern at global and regional scales (Govindasamy & Caldeira, 2000; Govindasamy et al., 2003; Bala et al., 2008; Caldeira & Wood, 2008; P. J. Irvine et al., 2016; Kravitz et al., 2013).

Here, five idealized model simulations are conducted to test the effectiveness of climate engineering using SRM. The results from the CO_2 simulation suggests that an increase in atmospheric carbon dioxide (CO_2) concentration will have a profound impact on the climate system and extreme events (Baker et al., 2018). Efforts to limit climate change and its risks, which require substantial and sustained reductions in greenhouse gas emissions to keep the global warming below 2^oC, are challenging because so little has been done so far and greenhouse gases continue to increase (Mach et al., 2016). However, our shading simulation results clearly show that SRM that offset atmospheric CO_2 concentrations could be used as an intermediate approach to counteract climate change and some of its adverse effects.

A 2.1% reduction in incoming sunlight, as simulated in the global uniform solar geoengineering experiment, largely offsets the global warming due to doubling of atmospheric CO_2, especially in the summer season. The winter warming is comparably less sensitive to solar geoengineering. Therefore, solar shading could result in a world with weaker seasonality, especially those over higher latitudes.

The regions with largest decrease in surface temperatures in the shaded climates are those that exhibited the most warming under the $2\times CO_2$ conditions, i.e., high-latitudes where strong positive feedbacks act on temperatures (Kravitz et al., 2013). Reductions in solar radiation favor cooling in the tropics, while CO_2 favours warming at higher latitudes (Govindasamy & Caldeira, 2000). The residual warming found in Global2.1 is consistent with earlier studies (Robock et al., 2008; Ricke et al., 2010), suggesting that the magnitude of compensation may vary, with residual changes larger in some regions than others. Residual warming is greatest in the polar regions during winter, as solar reduction has little impact on the winter polar regions.

Reducing solar radiation in the tropics could make tropical climates more habitable by reducing extremely high temperatures. It will also reduce local precipitation. We note that tropical shading also increases monsoon precipitation, especially in the northern hemisphere.

In addition, the 14% reduction in the polar regions will largely reduce the local warming caused by the doubled CO_2 concentration, especially in summer. This could help reduce the risk of impending polar ice sheet instability and subsequent sea level rise (e.g., Sutter et al. (2016)). However, we note that polar shading leads to increased storm activity at high latitudes.

The pattern in precipitation under the $2\times CO_2$ simulation suggests that the global hydrological cycle will be stronger (Held & Soden, 2006). Furthermore, there is a general poleward shift of the precipitation pattern caused by the atmospheric circulation (Yang et al., 2022). We find that shading is able to reduce the intensity of the hydrological cycle (Tilmes et al., 2013), even causing droughts, when solar radiation is too strong to fully offset mean global warming. A previous study found that the decrease in precipitation was due to the fundamental difference between the effects of CO_2 forcing and shading, which affect the thermal structure of the atmosphere (Cao et al., 2015).

Several climate simulations have shown significant downward trend in sea-ice extent through the 21st Century, especially during summer (J. Stroeve et al. (2007); J. C. Stroeve et al. (2012); Eisenman et al. (2011); Xia et al. (2014); Johannessen et al. (2004); Min et al. (2022)). According to Krishfield et al. (2014), the thick perennial ice cover has now been replaced by thinner first year ice. As sea-ice extent decreases during summer, more solar radiation is absorbed by the increased ocean area, heating the upper ocean and delaying the onset of ice growth. Polar shading may restore most of the sea ice, especially the summer sea ice.

A solar geoengineering approach aims to reduce climate risk. Here, we emphasize that an implementation could not change ocean acidification (Caldeira & Wickett, 2003). In addition, changes in rainfall might cause some risks in drought and heavy rainfall (P. Irvine et al., 2019). Besides the impact on regional climate change, ecosystems are affected by impacts on daily sunlight, also blocking harmful UV radiation (Teller et al., 2003).

5 Conclusions and Outlook

We have used idealised simulations to analyse the impacts of $2\times CO_2$ concentration on the climate and also evaluate the impacts of solar shading on global and regional climate. The $2\times CO_2$ world shows a global mean surface air temperature rise with strongest anomalies at high latitudes and over land. It also causes intensification and poleward shift of precipitation pattern, and a significant decrease in Arctic and Antarctic sea ice.

A global reduction in solar irradiance that fully offsets CO_2-driven warming would result in an overall reduction in the global hydrologic cycle and thus a reduction in precipitation, but with minor positive and negative anomalies in different parts of the globe. Reductions in solar radiation are most efficient in restoring temperature, seasonally in summer, regionally in low latitudes where background radiation is strong.

Using an alternative strategy, tropical solar reduction can prevent uninhabitable tropical warming. Meanwhile, it also weakens the intensity of ITCZ, while increases the monsoon in the subtropics. Polar solar reduction can largely offset the summer polar warming to prevent sea-ice loss and a possible long-term disintegration of the polar ice sheets. However, polar shading could lead to more storms at high latitudes. As a logical next step, more realistic experiments with detailed transient climate scenarios should be conducted to access the effectiveness of solar geoengineering and its effect on climate.

Acknowledgments

We are deeply grateful to all those who contributed to the success of this paper. We would like to thank our reviewers for their guidance, support and encouragement throughout the process. Their advice and expertise were critical in helping us shape the paper. We would also like to express our heartfelt thanks to the Alfred Wegener Institute, Helmholtz Centre for Polar and Marine Research, Bremerhaven, Germany, University of Bremen and the AWI Computing Centre for their support.

References

Angel, R. (2006). Feasibility of cooling the earth with a cloud of small spacecraft near the inner lagrange point (l1). *Proceedings of the National Academy of Sciences*, *103*(46), 17184–17189.

Applegate, P. J., & Keller, K. (2015). How effective is albedo modification (solar radiation management geoengineering) in preventing sea-level rise from the greenland ice sheet? *Environmental Research Letters*, *10*(8), 084018.

Baker, H. S., Millar, R. J., Karoly, D. J., Beyerle, U., Guillod, B. P., Mitchell, D., . . . Allen, M. R. (2018). Higher co2 concentrations increase extreme event risk in a 1.5 c world. *Nature Climate Change*, *8*(7), 604–608. doi: 10.1038/s41558-018-0190-1

Bala, G., Duffy, P., & Taylor, K. (2008). Impact of geoengineering schemes on the global hydrological cycle. *Proceedings of the National Academy of Sciences*, *105*(22), 7664–7669. doi: 10.1073/pnas.0711648105

Ban-Weiss, G. A., & Caldeira, K. (2010). Geoengineering as an optimization problem. *Environmental Research Letters*, *5*(3), 034009. doi: 10.1088/1748-9326/5/3/034009

Boer, G. (2011). The ratio of land to ocean temperature change under global warming. *Climate dynamics*, *37*(11), 2253–2270.

Brierley, C. M., Zhao, A., Harrison, S. P., Braconnot, P., Williams, C. J. R., Thornalley, D. J. R., … Abe-Ouchi, A. (2020). Large-scale features and evaluation of the PMIP4-CMIP6 midHolocene simulations. *Climate of the Past*, *16*(5), 1847–1872. doi: 10.5194/cp-16-1847-2020

Caldeira, K., Bala, G., & Cao, L. (2013). The science of geoengineering. *Annual Review of Earth and Planetary Sciences*, *41*. (https://doi.org/10.1146/annurev-earth-042711-105548) doi: 10.1146/annurev-earth-042711-105548

Caldeira, K., & Wickett, M. E. (2003). Anthropogenic carbon and ocean ph. *Nature*, *425*(6956), 365–365. Retrieved from `https://doi.org/10.1038/425365a` doi: 10.1038/425365a

Caldeira, K., & Wood, L. (2008). Global and arctic climate engineering: numerical model studies. *Philosophical Transactions of the Royal Society A: Mathematical, Physical and Engineering Sciences*, *366*(1882), 4039–4056. (https://doi.org/10.1098/rsta.2008.0132)

Cao, L., Bala, G., Zheng, M., & Caldeira, K. (2015). Fast and slow climate responses to co2 and solar forcing: A linear multivariate regression model characterizing transient climate change. *Journal of Geophysical Research: Atmospheres*, *120*(23), 12–037. doi: 10.1002/2015JD023901

CIESIN, S. (2015). Gridded population of the world, version 4 (gpwv4): population density. *Center for International Earth Science Information Network-CIESIN-Columbia University. NASA Socioeconomic Data and Applications Center (SEDAC). https://doi. org/10.7927/H4DZ068D*.

Council, N. R. (2015). *Climate intervention: Carbon dioxide removal and reliable sequestration.* National Academies Press. doi: 10.17226/18805

Crutzen, P. J. (2006). Albedo enhancement by stratospheric sulfur injections: A contribution to resolve a policy dilemma? *Climatic change*, *77*(3-4), 211. doi: 10.1007/s10584-006-9101-y

Curry, C. L., Sillmann, J., Bronaugh, D., Alterskjaer, K., Cole, J. N., Ji, D., … others (2014). A multimodel examination of climate extremes in an idealized geoengineering experiment. *Journal of Geophysical Research: Atmospheres*, *119*(7), 3900–3923. doi: 10.1002/2013JD020648

Dai, A., Luo, D., Song, M., & Liu, J. (2019). Arctic amplification is caused by sea-ice loss under increasing co2. *Nature communications*, *10*(1), 1–13.

Danilov, S., Sidorenko, D., Wang, Q., & Jung, T. (2017). The finite-volume sea ice–ocean model (fesom2). *Geoscientific Model Development*, *10*(2), 765–789.

Eisenman, I., Schneider, T., Battisti, D. S., & Bitz, C. M. (2011). Consistent changes in the sea ice seasonal cycle in response to global warming. *Journal of Climate*, *24*(20), 5325–5335. Retrieved from `https://doi.org/10.1175/2011JCLI4051.1` doi: 10.1175/2011JCLI4051.1

Glienke, S., Irvine, P. J., & Lawrence, M. G. (2015). The impact of geoengineering on vegetation in experiment g1 of the geomip. *Journal of Geophysical Research: Atmospheres*, *120*(19), 10–196.

Govindasamy, B., & Caldeira, K. (2000). Geoengineering Earth's radiation balance to mitigate CO2-induced climate change. *Geophysical Research Letters*, *27*(14), 2141–2144. doi: 10.1029/1999GL006086

Govindasamy, B., Caldeira, K., & Duffy, P. (2003). Geoengineering Earth's radiation balance to mitigate climate change from a quadrupling of CO2. *Global and Planetary Change*, *37*(1-2), 157–168. doi: 10.1016/S0921-8181(02)00195-9

Govindasamy, B., Thompson, S., Duffy, P. B., Caldeira, K., & Delire, C. (2002). Impact of geoengineering schemes on the terrestrial biosphere. *Geophysical Research Letters*, *29*(22), 18–1. doi: 10.1029/2002GL015911

Held, I. M., & Soden, B. J. (2006). Robust responses of the hydrological cycle to global warming. *Journal of climate*, *19*(21), 5686–5699.

Hu, Y., & Fu, Q. (2007). Observed poleward expansion of the hadley circulation since 1979. *Atmospheric Chemistry and Physics*, *7*(19), 5229–5236.

Irvine, P., Emanuel, K., He, J., Horowitz, L. W., Vecchi, G., & Keith, D. (2019). Halving warming with idealized solar geoengineering moderates key climate hazards. *Nature Climate Change*, *9*(4), 295–299. Retrieved from `https://doi.org/10.1038/s41558-019-0398-8` doi: 10.1038/s41558-019-0398-8

Irvine, P. J., Kravitz, B., Lawrence, M. G., & Muri, H. (2016). An overview of the earth system science of solar geoengineering. *Wiley Interdisciplinary Reviews: Climate Change*, *7*(6), 815–833. doi: 10.1002/wcc.423

Irvine, P. J., Lunt, D. J., Stone, E. J., & Ridgwell, A. (2009). The fate of the greenland ice sheet in a geoengineered, high co2 world. *Environmental Research Letters*, *4*(4), 045109.

Johannessen, O. M., Bengtsson, L., Miles, M. W., Kuzmina, S. I., Semenov, V. A., Alekseev, G. V., ... Cattle, H. P. (2004). Arctic climate change: observed and modelled temperature and sea-ice variability. *Tellus A: Dynamic Meteorology and Oceanography*, *56*(4), 328–341. Retrieved from `https://doi.org/10.3402/tellusa.v56i4.14418` doi: 10.3402/tellusa.v56i4.14418

Joshi, M. M., Gregory, J. M., Webb, M. J., Sexton, D. M., & Johns, T. C. (2008). Mechanisms for the land/sea warming contrast exhibited by simulations of climate change. *Climate dynamics*, *30*(5), 455–465.

Kageyama, M., Harrison, S. P., Kapsch, M.-L., Lofverstrom, M., Lora, J. M., Mikolajewicz, U., ... others (2021). The pmip4 last glacial maximum experiments: preliminary results and comparison with the pmip3 simulations. *Climate of the Past*, *17*(3), 1065–1089. Retrieved from `https://doi.org/10.5194/cp-17-1065-2021`

Kalidindi, S., Bala, G., Modak, A., & Caldeira, K. (2015). Modeling of solar radiation management: a comparison of simulations using reduced solar constant and stratospheric sulphate aerosols. *Climate Dynamics*, *44*(9), 2909–2925.

Kravitz, B., Caldeira, K., Boucher, O., Robock, A., Rasch, P. J., Alterskjær, K., ... Yoon, J. (2013). Climate model response from the geoengineering model intercomparison project (GeoMIP). *Journal of Geophysical Research: Atmospheres*, *118*(15), 8320–8332. (https://hal.archives-ouvertes.fr/hal-01091232)

Kravitz, B., MacMartin, D. G., Robock, A., Rasch, P. J., Ricke, K. L., Cole, J. N., ... others (2014). A multi-model assessment of regional climate disparities caused by solar geoengineering. *Environmental Research Letters*, *9*(7), 074013.

Krishfield, R. A., Proshutinsky, A., Tateyama, K., Williams, W. J., Carmack, E. C., McLaughlin, F. A., & Timmermans, M.-L. (2014). Deterioration of perennial sea ice in the beaufort gyre from 2003 to 2012 and its impact on the oceanic freshwater cycle. *Journal of Geophysical Research: Oceans*, *119*(2), 1271–1305. doi: 10.1002/2013JC008999

Lee, S. (2014). A theory for polar amplification from a general circulation perspective. *Asia-Pacific Journal of Atmospheric Sciences*, *50*(1), 31–43.

Lohmann, G., Butzin, M., Eissner, N., Shi, X., & Stepanek, C. (2020). Abrupt climate and weather changes across time scales. *Paleoceanography and Paleoclimatology*, *35*(9), e2019PA003782. (Special Section AGU Grand Challenges in the Earth and Space Sciences) doi: 10.1029/2019PA003782

Lu, J., Vecchi, G. A., & Reichler, T. (2007). Expansion of the hadley cell under global warming. *Geophysical Research Letters*, *34*(6). Retrieved from `https://doi.org/10.1029/2006GL028443` doi: 10.1029/2006GL028443

Lunt, D. J., Ridgwell, A., Valdes, P. J., & Seale, A. (2008). "sunshade world": A fully coupled gcm evaluation of the climatic impacts of geoengineering. *Geophysical Research Letters*, *35*(12). doi: 10.1029/2008gl033674

Mach, K. J., Mastrandrea, M. D., Bilir, T. E., & Field, C. B. (2016). Understanding and responding to danger from climate change: the role of key risks in the ipcc ar5. *Climatic Change*, *136*(3), 427–444.

MacMartin, D. G., Ricke, K. L., & Keith, D. W. (2018). Solar geoengineering as part of an overall strategy for meeting the 1.5 C paris target. *Philosophical Transactions of the Royal Society A: Mathematical, Physical and Engineering Sciences*, *376*(2119), 20160454. Retrieved from `https://doi.org/10.1098/rsta.2016.0454` doi: 10.1098/rsta.2016.0454

Matthews, H. D., & Caldeira, K. (2007). Transient climate–carbon simulations of planetary geoengineering. *Proceedings of the National Academy of Sciences*, *104*(24), 9949–9954.

McClellan, J., Keith, D. W., & Apt, J. (2012). Cost analysis of stratospheric albedo modification delivery systems. *Environmental Research Letters*, *7*(3), 034019. doi: 10.1088/1748-9326/7/3/034019

McCusker, K. E., Battisti, D. S., & Bitz, C. M. (2015). Inability of stratospheric sulfate aerosol injections to preserve the west antarctic ice sheet. *Geophysical Research Letters*, *42*(12), 4989–4997.

Min, C., Yang, Q., Chen, D., Yang, Y., Zhou, X., Shu, Q., & Liu, J. (2022). The emerging arctic shipping corridors. *Geophysical Research Letters*, e2022GL099157.

Moore, J. C., Jevrejeva, S., & Grinsted, A. (2010). Efficacy of geoengineering to limit 21st century sea-level rise. *Proceedings of the National Academy of Sciences*, *107*(36), 15699–15703.

Naik, V., Wuebbles, D. J., DeLucia, E. H., & Foley, J. A. (2003). Influence of geoengineered climate on the terrestrial biosphere. *Environmental Management*, *32*(3), 373–381.

Ricke, K. L., Morgan, M. G., & Allen, M. R. (2010). Regional climate response to solar-radiation management. *Nature Geoscience*, *3*(8), 537–541. (https://doi.org/10.1038/ngeo915)

Robock, A., Oman, L., & Stenchikov, G. L. (2008). Regional climate responses to geoengineering with tropical and arctic so2 injections. *Journal of Geophysical Research: Atmospheres*, *113*(D16). (https://doi.org/10.1029/2008JD010050)

Roose, S., Bala, G., Krishnamohan, K., Cao, L., & Caldeira, K. (2023). Quantification of tropical monsoon precipitation changes in terms of interhemispheric differences in stratospheric sulfate aerosol optical depth. *Climate Dynamics*, 1–16.

Shepherd, J. G. (2009). *Geoengineering the climate: science, governance and uncertainty.* Royal Society.

Shi, X., Lohmann, G., Sidorenko, D., & Yang, H. (2020). Early-Holocene simulations using different forcings and resolutions in AWI-ESM. *The Holocene*, *30*(7), 996–1015. doi: 10.1177/0959683620908634

Sidorenko, D., Goessling, H., Koldunov, N., Scholz, P., Danilov, S., Barbi, D., ... Jung, T. (2019). Evaluation of FESOM2. 0 coupled to ECHAM6. 3: preindustrial and HighResMIP simulations. *Journal of Advances in Modeling Earth Systems*, *11*(11), 3794–3815. Retrieved from `https://doi.org/10.1029/2019MS001696` doi: 10.1029/2019MS001696

Stroeve, J., Holland, M. M., Meier, W., Scambos, T., & Serreze, M. (2007). Arctic sea ice decline: Faster than forecast. *Geophysical research letters*, *34*(9). (https://doi.org/10.1029/2007GL029703)

Stroeve, J. C., Serreze, M. C., Holland, M. M., Kay, J. E., Malanik, J., & Barrett, A. P. (2012). The arctic's rapidly shrinking sea ice cover: a research synthesis. *Climatic change*, *110*(3), 1005–1027. (https://doi.org/10.1007/s10584-011-

0101-1)

Sutter, J., Gierz, P., Grosfeld, K., Thoma, M., & Lohmann, G. (2016). Ocean temperature thresholds for last interglacial west antarctic ice sheet collapse. *Geophysical Research Letters*, *43*(6), 2675–2682. doi: 10.1002/2016GL067818

Sutton, R. T., Dong, B., & Gregory, J. M. (2007). Land/sea warming ratio in response to climate change: Ipcc ar4 model results and comparison with observations. *Geophysical research letters*, *34*(2).

Teller, E., Hyde, R., Ishikawa, M., Nuckolls, J., & Wood, L. (2003). Active stabilization of climate: inexpensive, low-risk, near-term options for preventing global warming and ice ages via technologically varied solar radiative forcing. *University of California Lawrence Livermore National Laboratory*.

Tietsche, S., Notz, D., Jungclaus, J., & Marotzke, J. (2011). Recovery mechanisms of arctic summer sea ice. *Geophysical Research Letters*, *38*(2). doi: 10.1029/2010GL045698

Tilmes, S., Fasullo, J., Lamarque, J.-F., Marsh, D. R., Mills, M., Alterskjær, K., ... others (2013). The hydrological impact of geoengineering in the geoengineering model intercomparison project (geomip). *Journal of Geophysical Research: Atmospheres*, *118*(19), 11–036. doi: 10.1002/jgrd.50868

Van Aalst, M. K. (2006). The impacts of climate change on the risk of natural disasters. *Disasters*, *30*(1), 5–18.

Wang, Q., Danilov, S., Sidorenko, D., Timmermann, R., Wekerle, C., Wang, X., ... Schröter, J. (2014). The finite element sea ice-ocean model (fesom) v. 1.4: formulation of an ocean general circulation model. *Geoscientific Model Development*, *7*(2), 663–693.

Xia, W., Xie, H., & Ke, C. (2014). Assessing trend and variation of arctic sea-ice extent during 1979–2012 from a latitude perspective of ice edge. *Polar Research*, *33*(1), 21249. (https://doi.org/10.3402/polar.v33.21249)

Yang, H., Lohmann, G., Krebs-Kanzow, U., Ionita, M., Shi, X., Sidorenko, D., ... Gowan, E. J. (2020). Poleward shift of the major ocean gyres detected in a warming climate. *Geophysical Research Letters*, *47*(5), e2019GL085868. Retrieved from `https://doi.org/10.1029/2019GL085868` doi: 10.1029/2019GL085868

Yang, H., Lohmann, G., Lu, J., Gowan, E. J., Shi, X., Liu, J., & Wang, Q. (2020). Tropical expansion driven by poleward advancing midlatitude meridional temperature gradients. *Journal of Geophysical Research: Atmospheres*, *125*(16), e2020JD033158. Retrieved from `https://doi.org/10.1029/2020JD033158` doi: 10.1029/2020JD033158

Yang, H., Lu, J., Wang, Q., Shi, X., & Lohmann, G. (2022). Decoding the dynamic of poleward shifting climate zones using aqua-planet model simulation. *Climate Dynamics*. doi: 10.1007/s00382-021-06112-0

Zhang, Y., Held, I., & Fueglistaler, S. (2021). Projections of tropical heat stress constrained by atmospheric dynamics. *Nature Geoscience*, *14*(3), 133–137.

Zhang, Z., Moore, J. C., Huisingh, D., & Zhao, Y. (2015). Review of geoengineering approaches to mitigating climate change. *Journal of Cleaner Production*, *103*, 898–907. doi: 10.1016/j.jclepro.2014.09.076

Table 1: Simulations include pre-industrial control and 2×CO_2 climate that differ in atmospheric CO_2 content and the simulations in which solar insolation is reduced at various levels globally, or regionally at different latitudes over both hemispheres.

Simulation	CO_2 (ppm)	Region of insolation reduction	Insolation reduction (%)
piControl	284	-	-
2×CO_2	568	-	-
Global2.1	568	global	2.1
Tropical3.6	568	30^o N to 30^o S	3.6
Polar14	568	60^o N - 90^o N and 60^o S - 90^o S	14

Table 2: Global mean anomaly of incoming solar radiation, surface air temperature and precipitation in the climate changed simulations with respect to the piControl experiment. The anomalies are shown based on the last 100 years simulations for individual experiments. The error bars represent the standard deviation of anomalies.

	2×CO_2	Global2.1	Tropical3.6	Polar14
Solar Radiation	0.00%	-2.10%	-2.10%	-1.14%
Temperature	2.12±0.12	0.03±0.12	0.31±0.13	1.02±0.16
Precipitation	3.63±0.41%	-1.29±0.38%	-0.95±0.42%	1.73±0.41%

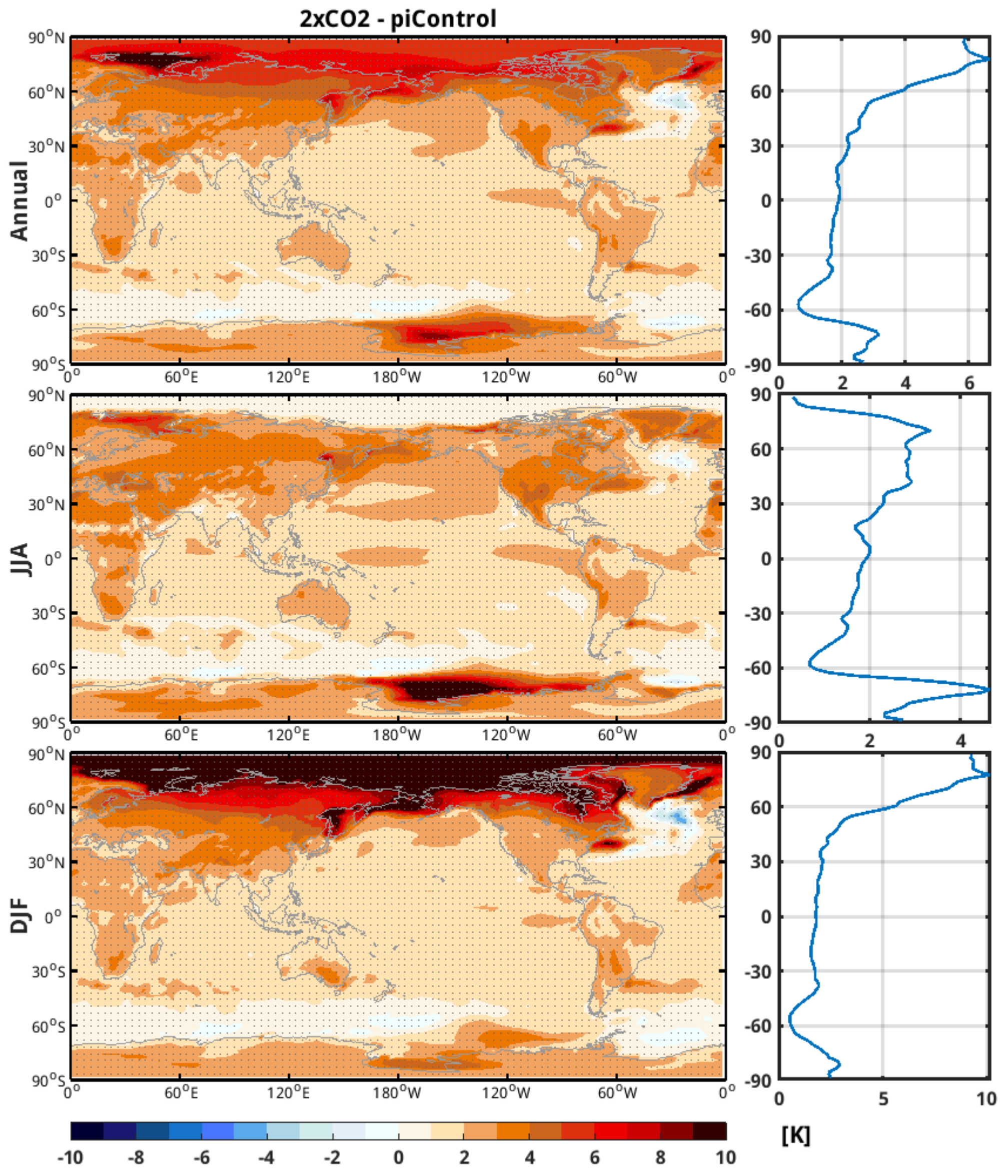

Fig. 1. Global surface air temperature anomalies for (a) Annual, (b) June-July-August (JJA) and (c) December-January-February (DJF) in the 2×CO_2 simulation with respect to the piControl simulation. Stippling indicates regions where the anomalies pass the 95% confidence level (two-tailed Student's t-test). The right panels show the zonal mean temperature anomaly.

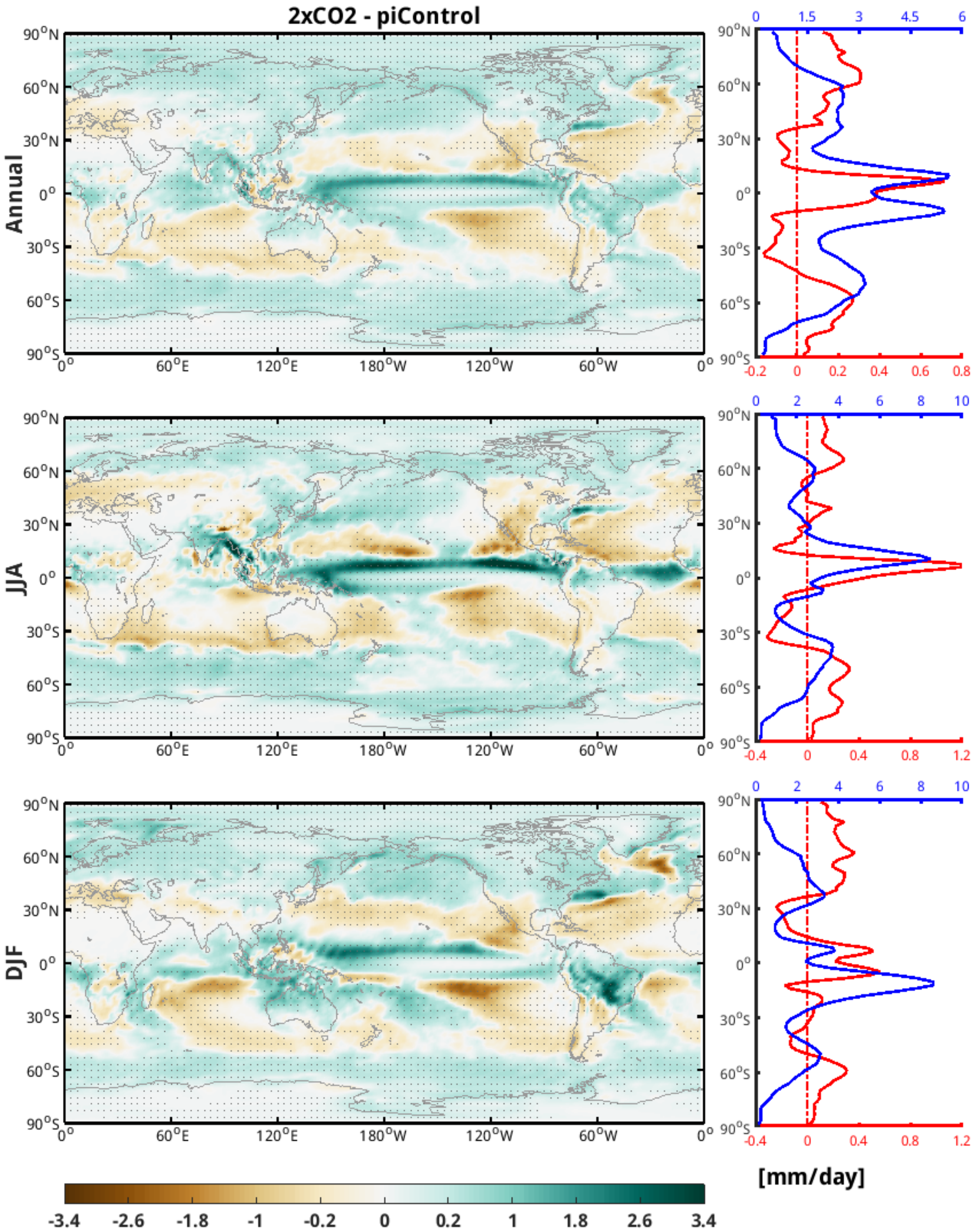

Fig. 2. Global Precipitation anomalies for (a) Annual, (b) June-July-August (JJA) and (c) December-January-February (DJF) in the $2\times CO_2$ simulation with respect to the piControl simulation. Stippling indicates regions where the anomalies pass the 95% confidence level (two-tailed Student's t-test). The right panels show the zonal mean precipitation climatology (blue) and the anomaly (red).

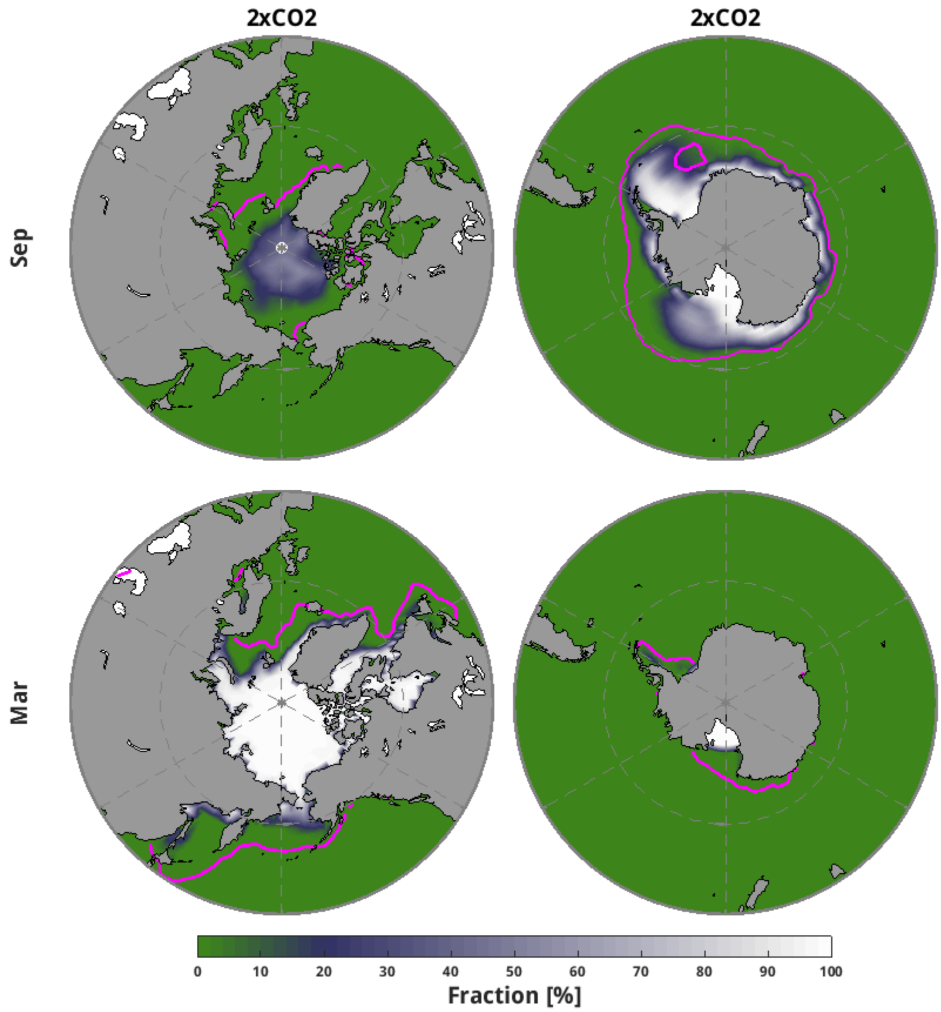

Fig. 3. (a) September and (b) March polar mean sea ice fraction in the $2\times CO_2$ simulation. Higher values are represented in white and lower values in dark blue, and ocean is represented by green colour. The pink contour lines represent the sea ice edge (5%) in the piControl experiment for comparison.

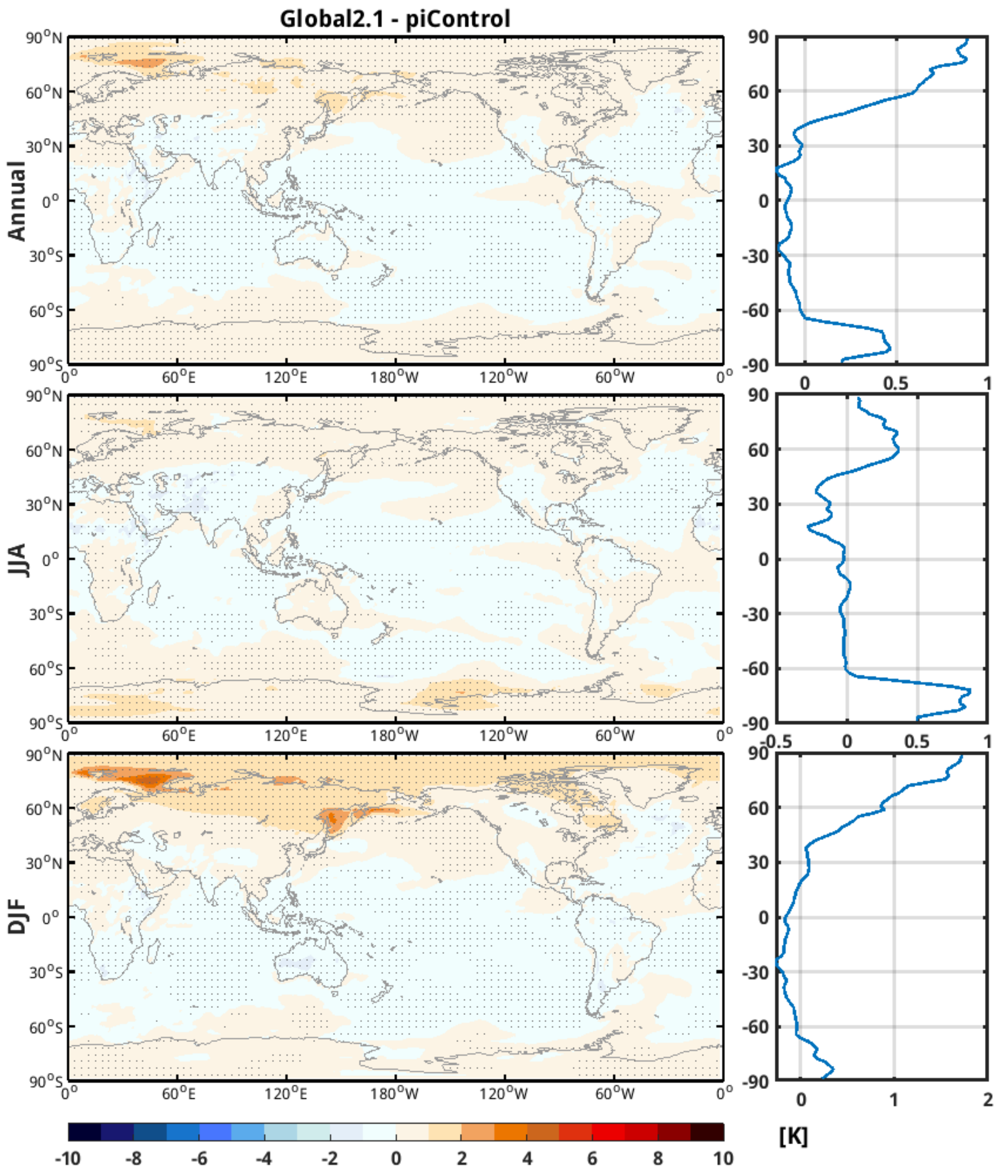

Fig. 4. Global surface air temperature anomalies for (a) Annual, (b) June-July-August (JJA) and (c) December-January-February (DJF) in the Global2.1 engineered simulation with respect to the piControl simulation. Stippling indicates regions where the anomalies pass the 95% confidence level (two-tailed Student's t-test). The right panels show the zonal mean temperature anomaly.

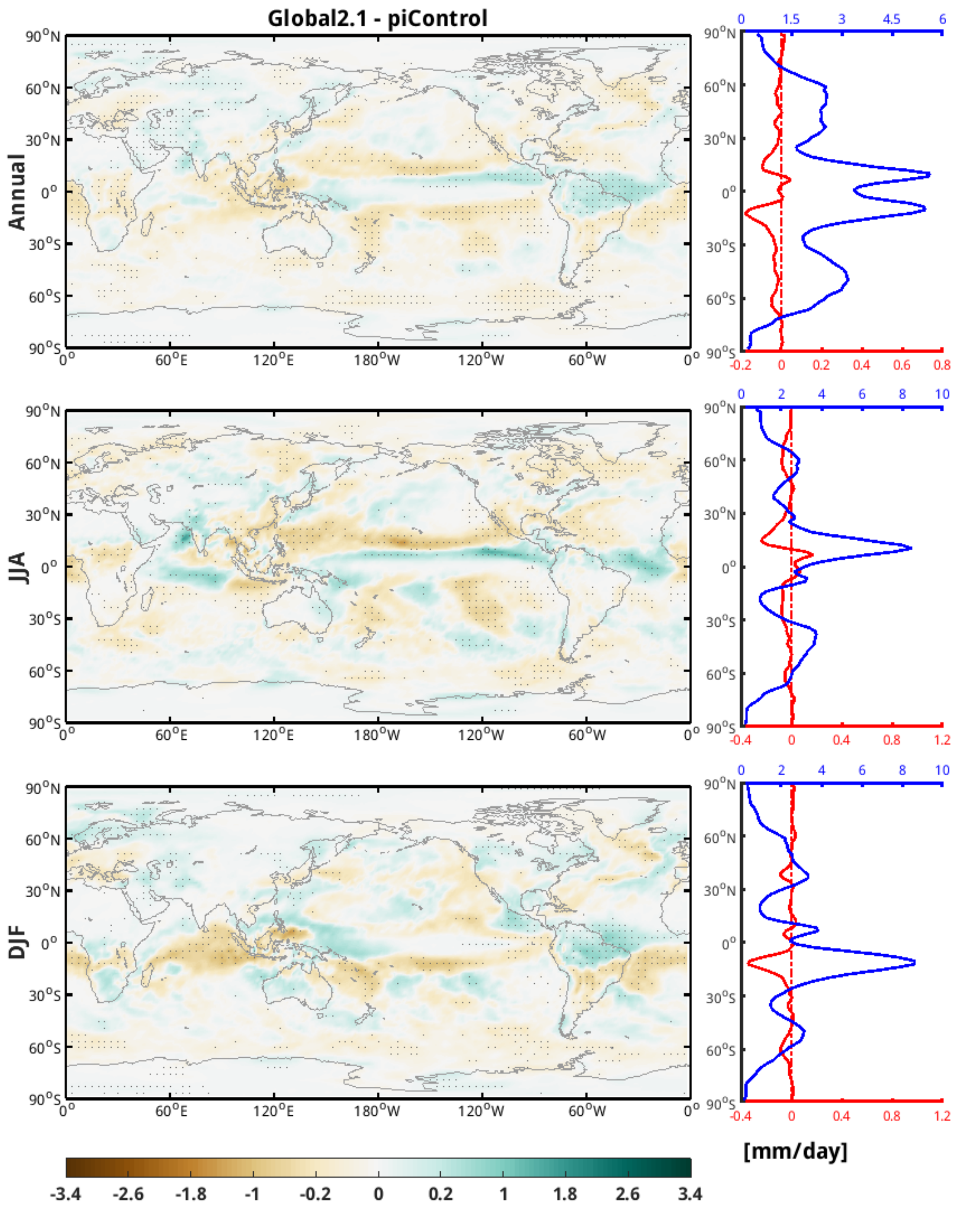

Fig. 5. Global Precipitation anomalies for (a) Annual, (b) June-July-August (JJA) and (c) December-January-February (DJF) in the Global2.1 engineered simulation with respect to the piControl simulation. Stippling indicates regions where the anomalies pass the 95% confidence level (two-tailed Student's t-test). The right panels show the zonal mean precipitation climatology (blue) and the anomaly (red).

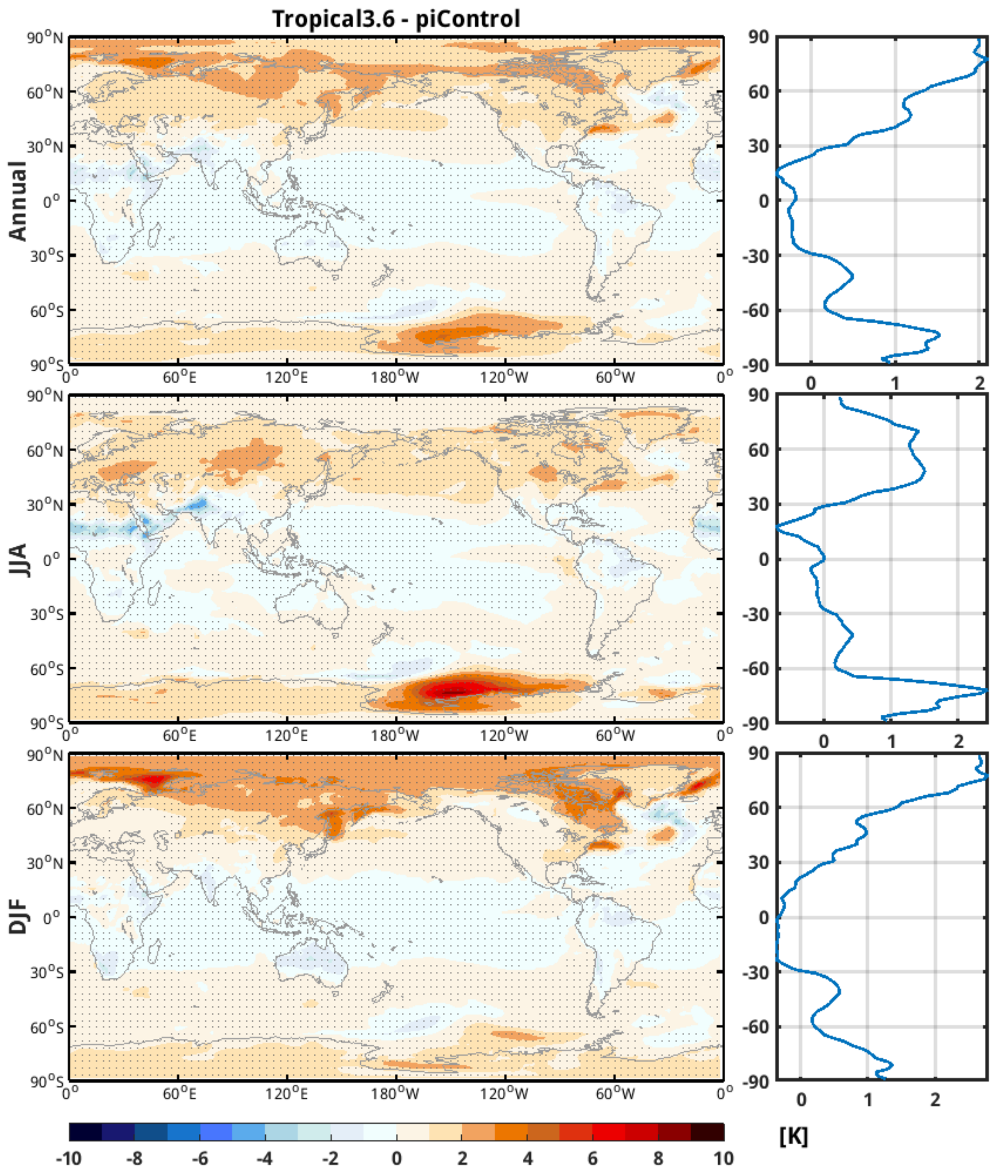

Fig. 6. Global surface air temperature anomalies for (a) Annual, (b) June-July-August (JJA) and (c) December-January-February (DJF) in the Tropical3.6 engineered simulation with respect to the piControl simulation. Stippling indicates regions where the anomalies pass the 95% confidence level (two-tailed Student's t-test). The right panels show the zonal mean temperature anomaly.

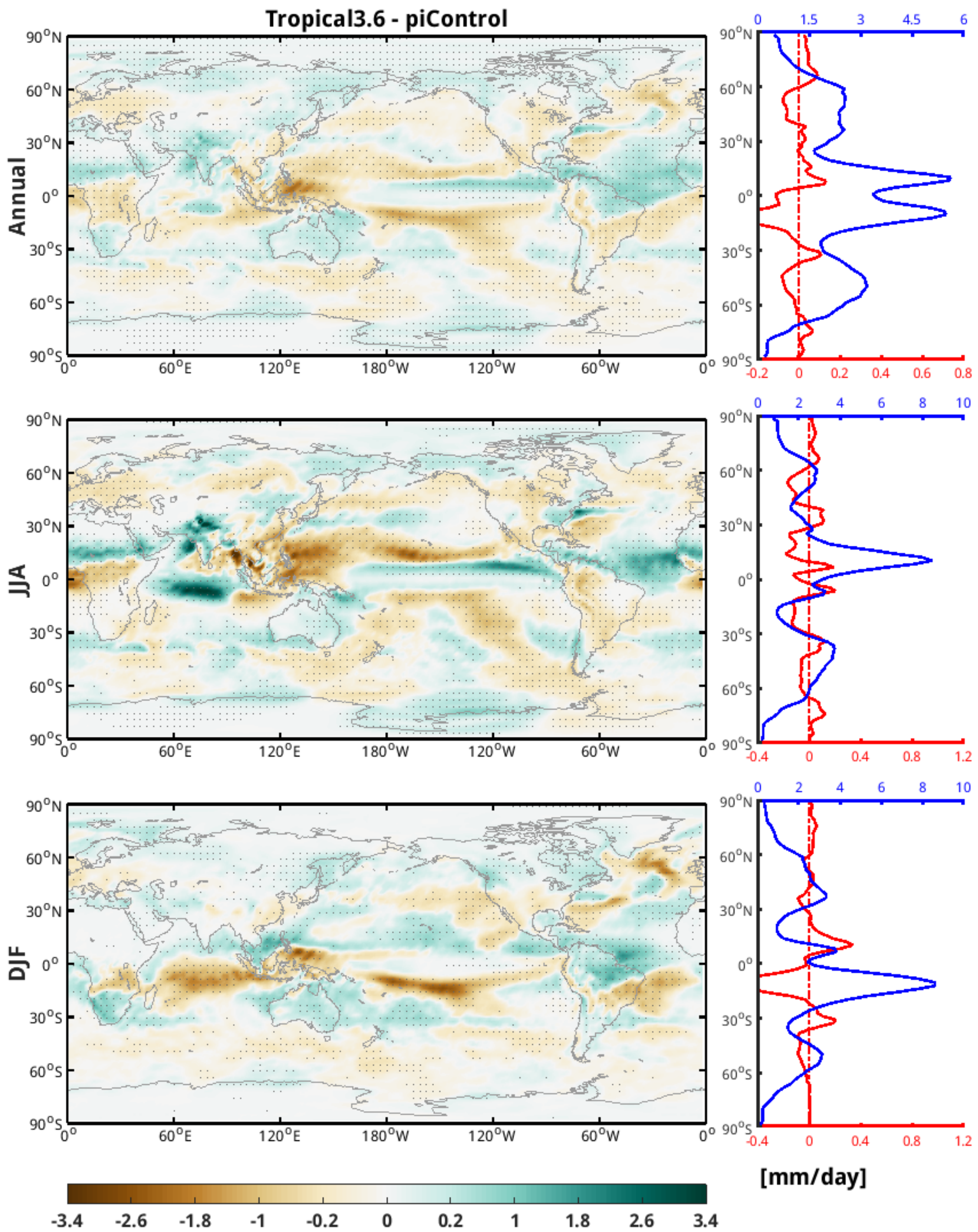

Fig. 7. Global Precipitation anomalies for (a) Annual, (b) June-July-August (JJA) and (c) December-January-February (DJF) in the Tropical3.6 engineered simulation with respect to the piControl simulation. Stippling indicates regions where the anomalies pass the 95% confidence level (two-tailed Student's t-test). The right panels show the zonal mean precipitation climatology (blue) and the anomaly (red).

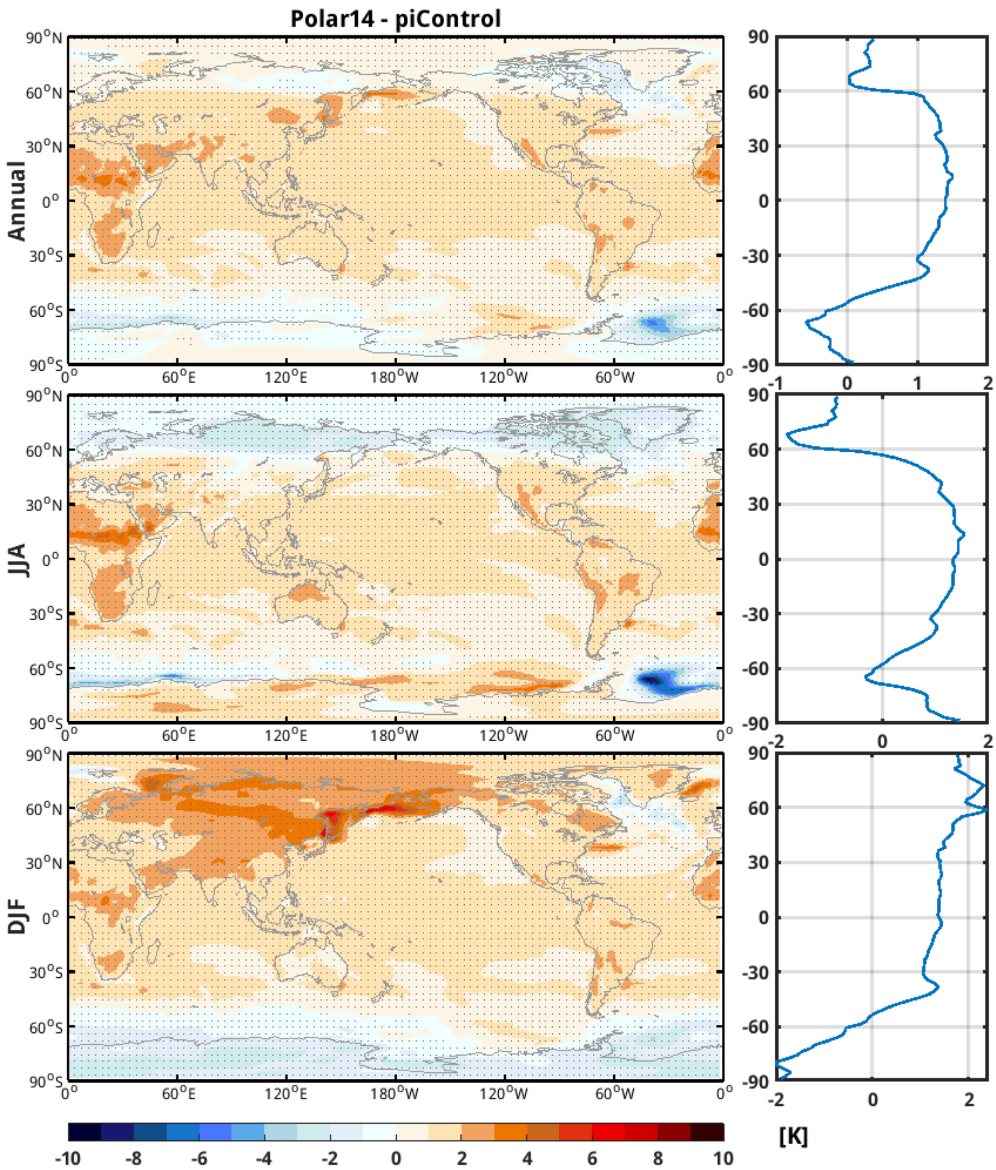

Fig. 8. Global surface air temperature anomalies for (a) Annual, (b) June-July-August (JJA) and (c) December-January-February (DJF) in the Polar14 engineered simulation with respect to the piControl simulation. Stippling indicates regions where the anomalies pass the 95% confidence level (two-tailed Student's t-test). The right panels show the zonal mean temperature anomaly.

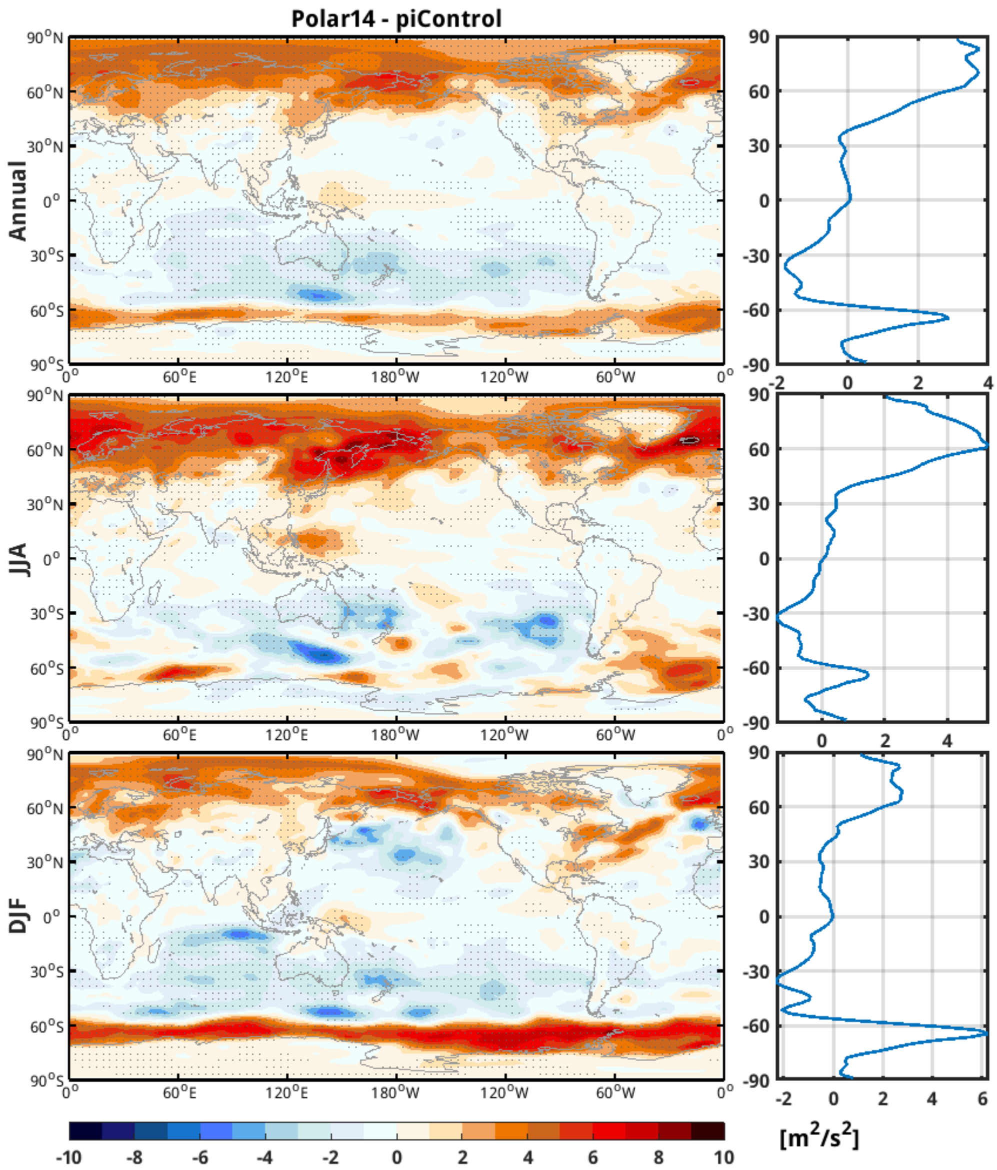

Fig. 9. Mean eddy kinetic energy (EKE) anomalies for (a) Annual, (b) June-July-August (JJA) and (c) December-January-February (DJF) in the Polar14 engineered simulation with respect to the piControl simulation. Stippling indicates regions where the anomalies pass the 95% confidence level (two-tailed Student's t-test). The right panels show the zonal mean temperature anomaly.

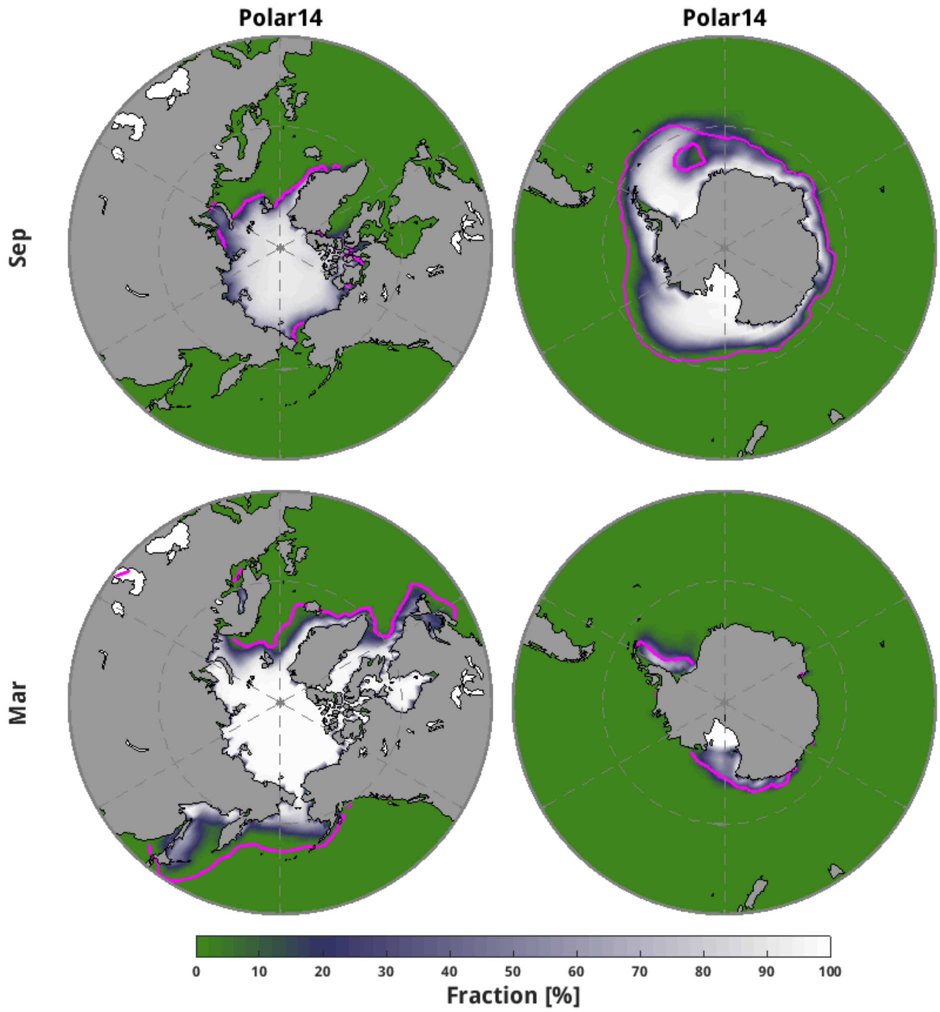

Fig. 10. (a) September and (b) March polar mean sea ice fraction in the Polar14 engineered simulation. Higher values are represented in white and lower values in dark blue, and ocean is represented by green colour. The pink contour lines represent the sea ice edge (5%) in the piControl experiment for comparison.